J Med Device. Author manuscript; available in PMC 2017 December 01.

Published in final edited form as:
J Med Device. 2017 June ; 11(2): . doi:10.1115/1.4035865.

Statistical Shape Modeling for Cavopulmonary Assist Device Development: Variability of Vascular Graft Geometry and Implications for Hemodynamics

Jan L Bruse[1], **Giuliano Giusti**, **Catriona Baker**, and **Elena Cervi**
Centre for Cardiovascular Imaging, UCL Institute of Cardiovascular Science & Great Ormond Street Hospital for Children

Level 6, Nurses Home, Great Ormond Street Hospital for Children, Great Ormond Street, London, WC1N 3JH, UK

Tain-Yen Hsia and **Andrew M Taylor**
Centre for Cardiovascular Imaging, UCL Institute of Cardiovascular Science & Great Ormond Street Hospital for Children

Level 7, Nurses Home, Great Ormond Street Hospital for Children, Great Ormond Street, London, WC1N 3JH, UK

Tain-Yen Hsia: tyhsia@virginmedia.com; Andrew M Taylor: a.taylor76@ucl.ac.uk

Silvia Schievano
Centre for Cardiovascular Imaging, UCL Institute of Cardiovascular Science & Great Ormond Street Hospital for Children

Level 6, Nurses Home, Great Ormond Street Hospital for Children, Great Ormond Street, London, WC1N 3JH, UK

Silvia Schievano: s.schievano@ucl.ac.uk

MOCHA Collaborative Group

Abstract

Patients born with a single functional ventricle typically undergo three-staged surgical palliation in the first years of life, with the last stage realizing a cross-like total cavopulmonary connection (TCPC) of superior and inferior vena cavas (SVC and IVC) with both left and right pulmonary arteries, allowing all deoxygenated blood to flow passively back to the lungs (Fontan circulation). Even though within the past decades more patients survive into adulthood, the connection comes at the prize of deficiencies such as chronic systemic venous hypertension and low cardiac output, which ultimately may lead to Fontan failure. Many studies have suggested that the TCPC's

[1]Centre for Cardiovascular Imaging, UCL Institute of Cardiovascular Science & Great Ormond Street Hospital for Children, London, UK, jan.bruse.12@ucl.ac.uk.

Competing Interests
All authors declare no relationships or activities that could appear to have influenced the submitted work and declare no competing interest.
This report incorporates independent research from the National Institute for Health Research Biomedical Research Centre Funding Scheme. The views expressed in this publication are those of the author(s) and not necessarily those of the NHS, the National Institute for Health Research or the Department of Health.

inherent insufficiencies might be addressed by adding a cavopulmonary assist device (CPAD) to provide the necessary pressure boost. While many device concepts are being explored, few take into account the complex cardiac anatomy typically associated with TCPCs. In this study, we focus on the extra cardiac conduit vascular graft connecting IVC and pulmonary arteries as one possible landing zone for a CPAD and describe its geometric variability in a cohort of 18 patients that had their TCPC realized with a 20mm vascular graft. We report traditional morphometric parameters and apply statistical shape modeling to determine the main contributors of graft shape variability. Such information may prove useful when designing CPADs that are adapted to the challenging anatomical boundaries in Fontan patients. We further compute the anatomical mean 3D graft shape (template graft) as a representative of key shape features of our cohort and prove this template graft to be a significantly better approximation of population and individual patient's hemodynamics than a commonly used simplified tube geometry. We therefore conclude that statistical shape modeling results can provide better models of geometric and hemodynamic boundary conditions associated with complex cardiac anatomy, which in turn may impact on improved cardiac device development.

Introduction

Children born with only one functional pumping chamber of the heart (single ventricle, SV) typically need to undergo three stages of surgical palliation in the first years of life. The last of these stages that creates the *Fontan* circulation, aims at providing blood flow to the systemic and pulmonary circulation using only the SV, without requiring an additional second pumping ventricle [1,2]. This is achieved by directly connecting the superior and inferior vena cavas (SVC and IVC) to the right and left pulmonary arteries (RPA and LPA) creating a total cavopulmonary connection (TCPC), allowing all systemic venous return (deoxygenated blood) to passively flow back to the lungs.

While short- and mid-term outcomes have improved over the past decades [2] more and more patients survive into adulthood and have to live with this inherently inefficient Fontan circulation, often associated with chronic systemic venous hypertension, low cardiac output (CO), impaired exercise capacity and high risk for thromboembolism and arrhythmia, which ultimately may lead to organ failure [1–4]. As there is a constant shortage in organ donors, it has been proposed to use (mechanical) cavopulmonary assist devices (CPAD) as an additional pumping source providing a 3-5mmHg pressure boost to restore normal cavopulmonary pressure levels [5–7]. Current CPAD design concepts range from micro-axial [6,8–11] and propeller [12] blood pumps to viscous impeller pumps [7,13–15] or pneumatic [16] and shape memory contraction solutions [17]. Yet, particularly in cases of complex congenital cardiac malformations, device developers face one key challenge: complex cardiac anatomy, which poses geometric constraints for device dimensions, placement and function.

The generic TCPC, using an extra cardiac conduit (ECC) vascular graft to connect IVC with SVC and pulmonary arteries (PAs) is often depicted as a simple, quasi-rectangular cross (Fig. 1a). However, assessing post-Fontan anatomy using modern medical imaging techniques such as cardiovascular magnetic resonance (CMR), TCPC anatomy is highly

variable [18] and at times far from cross-like (Fig. 1b). Nevertheless, most studies focusing on CPAD development employ simplified tubular cross connections as TCPC approximation for both *in-vitro* and *in-silico* testing [7,9–11,13–15,19].

With this study, we aim to raise the awareness of the high shape variability of TCPC anatomy, which we believe should be taken into account for CPAD development. We sought to demonstrate how statistical shape modeling (SSM) prior to actual device design and testing can help determine principal contributors to anatomic variability, which can then be taken into account during the device development process. The general aim would be to design a device that fits well the majority of the population, despite its anatomic variability.

As SVC and PA shape and configuration typically vary substantially making device deployment and fixation difficult, we deem the ECC graft – being made of man-made, implantable material that does not grow with the patient – to be more suitable for CPAD placement. However, even vascular graft geometry varies between patients due to different anatomical configurations (e.g. space between dilated SV and PAs, compressing aorta [20], body size differences etc.) and a simple, straight tube may not be a sufficient approximation when designing a CPAD to be placed in the graft. Therefore, we focus in this paper on the geometric variability of the ECC graft and present traditional morphometric parameters of a cohort of 18 patients post-Fontan with a TCPC connection via ECC graft. We apply statistical shape modeling (SSM) [21] with Principal Component Analysis (PCA) to describe principal contributors to three-dimensional (3D) graft shape variability [22]. As a first approximation of characteristic shape features of our graft population, we compute a 3D anatomical mean shape (the so-called *template*), which is written out as an STL file that can directly be used in *in-vitro* (via 3D printing) and *in-silico* testing.

We hypothesized that developing a CPAD using the template graft will fit better the majority of the population and hence, yield more realistic hemodynamic performance (i.e. in terms of pressure drop) than previously used simplified tubular structures. In order to test if the average graft indeed represents average population hemodynamics better, Computational Fluid Dynamic (CFD) was performed on all 18 patient grafts as well as on the template graft and a simple tube. We then quantified how much the template graft's gross flow characteristics deviate from each individual patient graft's flow and whether it makes a statistically significant difference to use the geometry of the computed template graft instead of approximating graft geometry with a tube.

Methods

Patient Population

A total of 18 SV patients (mean age 15.8±4 years) who underwent routine CMR examination at our center 8.4±3.4 years after Fontan (TCPC) completion were retrospectively analyzed in this study. Patients had different initial primary diagnoses of SV congenital heart defects (Table 1), but all underwent completion of the Fontan circulation. Only patients with pure (i.e. not converted from another connection type) ECC Fontan connection were included. In all patients, the connection between IVC and PAs had been realized via a 20mm GoreTex (W. L. Gore & Associates Inc., Newark, DE) vascular graft.

Ethical approval was obtained from the UCL Institute of Child Health/Great Ormond Street Hospital for Children Research Ethics Committee, and all patients or legal parent or guardian gave informed consent for research use of the data.

Image Processing

Three-dimensional volumes of the Fontan connection were obtained from CMR using a 1.5T Avanto MR scanner (Siemens Medical Solutions, Erlangen, Germany) with a 3D balanced, steady-state free precession (bSSFP), whole-heart, free breathing isotropic sequence (isovolumetric voxel size 1.5mm x 1.5mm x 1.5mm). IVC blood flow was derived from phase contrast magnetic resonance (PC-MR) imaging, acquired and averaged over one cardiac cycle at rest.

Three-dimensional models of the ECC grafts were segmented and reconstructed semi-automatically using Active Contours segmentation tools in ITKSnap by one operator [23]. The models were cut consistently as close as possible to the PAs at the level of graft anastomosis and below, parallel to the diaphragm, at the level where the hepatic veins join the IVC (Fig. 2), thereby defining the maximum possible graft length that could be used for CPAD placement.

The cut patient graft models were exported as STL (stereolithography) computational surface meshes from ITKSnap (Fig. 3) and were smoothed using a passband filter within the *vmtksurfacesmoothing* function prior to further analysis.

Morphometry

Three-dimensional morphometry of the graft models was performed using automated tools of The Vascular Modeling Toolkit (VMTK, *www.vmtk.org*, [24]) in combination with Matlab (The Mathworks, Natick, MA). Using VMTK's *vmtkcenterline* and *vmtksurfacemassproperties* functions, the centerline length L_{CL}, the centerline tortuosity L_t and average curvature C_{av}, the graft model volume V, and the maximum, minimum and average inscribed sphere diameter along the graft centerline D_{max}, D_{min} and D_{av} were extracted for all models [25,26].

Statistical Shape Model

Background—To obtain the mean (i.e. averaged) 3D graft geometry of our cohort, we used the non-parametric statistical shape modeling (SSM) framework *Deformetrica* [27] (*www.deformetrica.org*). It simultaneously computes the so-called *template* or mean anatomical shape of a shape population and its *deformations* towards each subject shape by modeling input shapes provided as surface meshes as so-called *mathematical currents* [28]. This approach does not require point-to-point correspondence between input shapes and is thus attractive for the analysis of cardiac anatomy [29]. To model shapes non-parametrically, surface meshes need to be transferred into a vector space of currents, which is generated by two Gaussian kernels. In this way, shapes are described as a collection of shape features, rather than actual point coordinates. The smooth and invertible deformations registering the computed template towards each subject shape are estimated using the *Large Deformation Diffeomorphic Metric Mapping* (LDDMM) framework [30]. These deformations,

parameterized by the resulting sets of deformation vectors ϕ describe all 3D shape variability within the population. The theoretical background for the SSM method is provided by the cited literature and a detailed user guide including validation with traditional morphometrics is given in [31].

Setup and description of shape variability via Principal Component Analysis (PCA)—Prior to shape analysis in Deformetrica, graft models were rigidly aligned using an Iterative Closest Point (ICP) algorithm in VMTK [32]. For the following analyses, variability introduced by varying graft alignment in space was removed following a Generalized Procrustes Analysis (GPA), which iteratively re-aligns objects to the computed template shape until convergence [31,33].

The two principal parameters to be set by the user are the two kernel widths λ_W and λ_V, related to describing surface shapes as mathematical currents [31]. Here, λ_W and λ_V were set to 5mm and 15mm, respectively, allowing non-rigid registration of the template to each subject graft shape with low matching errors. Deformetrica then simultaneously computes the 3D template graft shape and writes out the subject-specific deformation vectors ϕ_i, mapping the template shape towards each patient graft shape i (for $i \in [1, 2, \ldots, 18]$).

Those sets of vectors essentially represent a numerical description of all 3D shape variability within the dataset and were thus used for further analysis using *Principal Component Analysis* (PCA, [34]). Using the covariance matrix of the combined ϕ_i, the main modes of deformation were extracted using Matlab as explained in [35] and [36], starting from the first shape mode, which accounts for the largest percentage of shape variability, until 90% of the total variability was explained. The graft shape variations described by the extracted PCA shape modes were visualized as deformations of the template along the respective mode in ParaView [37] (*www.paraview.org*) from –3 to +3 standard deviations (SD). All computed graft shapes (i.e. the template and its PCA shape mode deformations) were written out as VTK/STL surface mesh files.

Furthermore, *PCA shape vectors* containing the subject-specific PCA shape mode loadings for each mode (scalar product between ϕ_i and kth PCA shape mode) were derived by projecting each patient graft shape onto the obtained PCA shape modes as detailed in [31,36]. In this way, a low-dimensional numerical description of each patient's 3D graft shape was obtained, which was used for further bivariate correlation analysis in order to quantitatively assess associations between PCA shape modes and the chosen morphometric parameters.

The template and deformation computation was run on a 32GB workstation, using 16 cores in parallel, resulting in computation times of about 4 hours. The template was validated via 9-fold cross validation and geometrically as mean graft shape by comparing its 3D morphometrics (L_{CL}, V, D_{av}) to the mean values of those parameters derived from the population, as detailed in [31].

Computational Fluid Dynamics (CFD) simulations

CFD simulations of blood flow through the graft models were performed using ANSYS Fluent v17 (Ansys Inc., Canonsburg, PA). Simulations were run for all 18 patient grafts as well as for the computed template graft and for a tube of 20mm diameter and same length as the template graft (70.5mm), which would commonly be used for CPAD development as an approximation of IVC/vascular graft geometry. All 20 graft simulations were set up with the same boundary conditions of $\dot{V}_{in}$=2.58l/min inflow at the level where the IVC was cut (inlet, Fig. 4) and a fixed pressure of p_{outlet}=11mmHg at the level of the PAs (outlet).

Those conditions were set based on the average measured IVC flow in our cohort and typical Fontan pressures reported previously [38]. Prior to CFD analysis, graft models were fitted with tubular flow extensions of length 5 times the inlet diameter. Each graft volume was discretized with a centerline-adaptive unstructured tetrahedral mesh with an average size of ~630.000 cells, following a mesh independence study. Meshing was performed using VMTK and ICEM CFD (Ansys Inc., Canonsburg, PA). Flow conditions were assumed to be laminar and blood was modeled as an incompressible Newtonian fluid with constant density ρ=1060kg/m^3 and constant viscosity μ=3.6mPas. The velocity and pressure field within the graft models was computed until physical and numerical convergence (residuals <10e-05). To assess gross flow characteristics, averaged pressure at the inlet and outlet was monitored and the pressure drop across the graft Δp was computed and recorded for each model. CFD results, such as pressure maps, were derived and visualized in CFD-Post (Ansys Inc., Canonsburg, PA).

Statistical Analysis

For each patient graft model i, the absolute deviation in pressure drop $Dev_{template,i}$ between the computed pressure drop of the template graft $\Delta p_{template}$ and the individual pressure drop $\Delta p_{graft,i}$ was computed as follows (Eq. 1):

$$Dev_{template,i}=\mathrm{abs}(\Delta p_{template}-\Delta p_{graft,i})/\Delta p_{graft,i})\cdot 100\% \quad (1)$$

Similarly, the deviation $Dev_{tube,i}$ between the pressure drop of the simple tube Δp_{tube} and each individual pressure drop $\Delta p_{graft,i}$ was computed as follows (Eq. 2):

$$Dev_{tube,i}=\mathrm{abs}((\Delta p_{tube}-\Delta p_{graft,i})/\Delta p_{graft,i})\cdot 100\% \quad (2)$$

with $\Delta p_{template}$ being the pressure drop obtained from the CFD simulation of the template graft shape, Δp_{tube} being the pressure drop computed for the 20mm diameter tube and $\Delta p_{graft,i}$ being the pressure drop across each patient graft model. Mean deviations and confidence intervals are reported to determine how much each model used to approximate the population (template or simple tube) on average deviates from the actual pressure drop across each patient graft. The distributions of $Dev_{template,i}$ and $Dev_{tube,i}$ were then compared using Wilcoxon Signed Rank test to determine whether it makes a significant difference to

use either template or tube when approximating population hemodynamics. Further, 95% confidence intervals (95CI) are reported for all parameters.

To investigate associations between PCA shape modes and chosen morphometric parameters, standard bivariate correlation analysis was used, reporting Pearson's correlation coefficient r for normally distributed and Kendall's τ for non-normally distributed input data. Normality was assessed using the Shapiro-Wilk test. Results were considered to be statistically significant at level $p < .05$. All statistical tests were performed using IBM SPSS Statistics (SPSS Inc., Chicago, IL).

Results

Morphometry

For each patient graft model, individual values as well as averages and standard deviations for the measured geometric parameters L_{CL}, L_t, C_{av}, V and the diameters along the centerline D_i are reported in Table 2. The 95CI for graft length L_{CL} was 65.3mm to 77.3mm, for the graft volume V 17.6ml to 22.3ml, for the maximum diameter along the centerline D_{max} 17.5mm to 19.2mm, for the minimum diameter D_{min} 13.4mm to 14.6mm, and for the average diameter D_{av} 15.7mm to 16.8mm.

Statistical Shape Model

Computed 3D template graft shape—The template graft shape visually integrated key shape features of the patient grafts within our population such as a slightly bended, c-shaped overall graft geometry combined with a slight bend and flaring towards the PA anastomosis site (Fig. 5).

Its graft length $L_{CL,t}$ was 70.5mm, volume V_t was 19.4ml and average diameter along the centerline $D_{av,t}$ was 16.7mm. Those values were within the 95CIs obtained from traditional morphometry on our 18 patient graft models and showed overall very low deviation from the mean population values for L_{CL}, V and D_{av} (-1.1%, -2.5% and +3.0%, respectively), validating the computed template shape as a good approximation of the mean or averaged 3D graft shape (Table 3). Following the 9-fold cross validation, the computed template graft shape was stable with low surface distance errors of 0.105±0.026mm on average (Fig. 6). The computed template graft will be made publicly available for device developers.

Shape modes derived from PCA as descriptors of 3D graft shape variation—PCA on the deformation vectors ϕ_i extracted 10 shape modes, accounting for over 90% of total shape variability (Fig. 7). Here, we focus on the first three shape modes (accounting for 55.8% of the total), as further modes only accounted for a negligible percentage of shape variability.

PCA shape mode 1 (accounting for 29.5% of variability), visually mainly described graft shape variability related to differences in graft *length* and size as shown in Fig. 8a. Thereby, graft geometry varied from short and compact to stretched and elongated grafts that show a distinct flaring towards both the IVC as well as the PA anastomosis sites. It was significantly associated with changes in L_{CL} ($r = 0.795$, $p < .001$), V ($r = 0.897$, $p < .001$) and D_{max} ($\tau =$

0.451, $p = .009$). Further correlation p-values for all morphometric parameters are provided in Table 4.

PCA shape mode 2 (accounting for 16.2% of variability, Fig. 8b) visually related to the *curvature* or bending of the graft, ranging from relatively straight to more curved, c-shaped graft geometries that show a subtle flaring at the location of PA anastomosis. Numerically, shape mode 2 was significantly associated with changes in L_t ($\tau = 0.569$, $p = .001$), C_{av} ($\tau = 0.346$, $p = .045$), D_{max} ($\tau = -0.490$, $p = .004$) and D_{av} ($r = -0.571$, $p = .013$), confirming the visual results (Table 4).

Finally, PCA shape mode 3 (accounting for 10.1% of variability, Fig. 8c) visually described graft shape variability associated with differences in graft *diameter*, showing similar graft curvature and length for both extremes (±3 SD), but an overall slightly thinner and thicker graft, respectively. However, associations with morphometric parameters were not statistically significant (Table 4).

Computational Fluid Dynamics

Volume-rendered pressure maps for each of the patient grafts, the computed template graft and the tube geometry are shown in Fig. 9. For the patient graft models, local pressure distributions visually varied from patient to patient and differed substantially from the pressure map computed for the tube. The pressure map derived for the computed template shape though comprised features closer to the individual patient pressure distributions.

The mean pressure drop from IVC to PA anastomosis site averaged over the 18 grafts $\Delta_{\text{pgraft, av}}$ was 0.187mmHg (with 95CI 0.161mmHg to 0.212mmHg). The computed pressure drop in the template graft, $\Delta p_{template}$ was 0.150mmHg and thus slightly underestimated (by 20%) the actual mean pressure drop derived from the population. Yet, the tube with 20mm diameter and length 70.5mm (same as computed template) underestimated the pressure drop by 73%, with Δ_{ptube} computed as 0.050mmHg (Table 3).

Looking to the individual pressure drops (Table 2), $\Delta p_{template}$ deviated from the individual $\Delta p_{graft,i}$ on average by $Dev_{template,i} = 28.4\%$ (95CI 19.9% to 36.9%), whereas the tube pressure drop Δp_{tube} deviated on average by $Dev_{tube,i} = 70.4\%$ (95CI 65.1% to 75.7%), which was a significantly higher deviation for the simple tube ($p<.001$, Fig. 10).

Discussion

With about 800-1000 patients annually receiving three-staged Fontan palliation in the US [3], broadening indications for the operation [2] and more patients surviving into adulthood [4], the number of patients living with total cavopulmonary connections is increasing. The Fontan circulation however, comes with inherent deficiencies such as systemic venous hypertension, which ultimately can lead to Fontan or organ failure. Recent studies therefore suggest a four-staged rather than a three-staged surgical pathway, with the fourth stage consisting of a right-sided ventricular assist device as bridge-to-transplant or bridge-to-recovery [3]. Hence, it is crucial to exploit current state-of-the-art engineering tools in device development to explore options for an improved, economical CPAD design.

One possible landing zone for a CPAD could be the ECC graft, which although manmade, still varies considerably depending on the anatomical configuration of the patient. Here, we measured geometric parameters such as lengths and diameters of ECC graft models reconstructed from CMR data in a cohort of 18 SV patients to describe graft shape variability and provide boundary values for suitable CPAD dimensions. Previous studies have assessed graft cross-sectional area and diameters; however, relying on two-dimensional, manual measurements using cardiac catheterization images [39,40]. We believe that our study presents geometric data of the largest cohort of patients with 20mm ECC grafts assessed via CMR to date.

Further, we present the first statistical shape model of an ECC graft population and found graft length, curvature and diameter to be the principal geometric contributors to shape variability as visualized and quantified via PCA. Determining such key elements of anatomic variability prior to device development may contribute to the design of better fitting devices that already take into account challenging anatomical boundary conditions typical for a specific patient population.

We further computed the mean graft shape model (template graft), which comprised key 3D shape features of our input population. We hypothesized that such a mean shape can serve as good initial approximation of population anatomy, resulting in more realistic geometric and hemodynamic boundary conditions that will be beneficial for device development.

CFD simulations showed that the computed template graft visually captured well local flow features found in individual graft geometries and in addition yielded a reasonable approximation of the actual mean pressure drop averaged over all 18 patients. A simplified tube geometry, as often employed for initial device design, however, underestimated the average pressure drop across the graft by 73% when compared to the average of the population.

To assess whether the computed template graft also better performs when approximating an individual patient's hemodynamics, we quantified how much the template graft's pressure drop deviates from each individual patient graft's pressure drop and compared results with those of the tube geometry. Our results confirmed that the computed mean 3D graft shape yields a significantly better approximation of actual individual hemodynamic performance than the simplified model ($p < .001$). This, for the first time, proved that such a computed mean shape even in the case of relatively confined shape variability of ECC grafts overall performs much better than a simplified tube geometry.

The computed template model will be provided as a downloadable STL file, which can be used for more realistic *in-vitro* testing or *in-silico* hemodynamic or CPAD deployment simulations. As TCPC anatomical configurations are highly variable, we believe that computed 3D mean shapes (templates) of cardiac anatomy could provide a solution to avoid cost-intensive patient-specific device development, but help focus on devices that adapt to average anatomical constraints, representative of the majority of the population. Future studies may also take into account the computed PCA shape mode results by using the extreme shapes of the modes (±3SD) as geometric boundaries to cover an even wider range

Europe PMC Funders Author Manuscripts

of likely anatomy. By applying clustering techniques, subgroups within a patient population could be identified in order to adopt a more economical "few-sizes-fit-all" approach for device development. Particularly for complex cardiac anatomy, this could be an appealing solution.

While previous studies combined statistical shape modeling and computational fluid dynamics mainly to speed-up patient-specific blood flow simulations [41,42] or to generate improved idealized shapes [43], to the best of our knowledge, this is the first study combining those techniques to assess hemodynamic performance of a computed template shape compared to population and individual hemodynamics in the context of cardiac device development.

Limitations

A major limitation of our study is the relatively small sample size of SV patients with ECC grafts. One could imagine graft geometry to vary even more once more patients are included so that our mean graft model may not approximate all of them well. However, we are confident that graft shape would most likely vary according to the derived principal shape modes in length, curvature and diameter. In addition, it is still challenging to obtain usable CMR data of a consistent patient cohort that present TCPCs with the same graft type.

Secondly, we only assessed the pressure drop across the graft as one single, gross flow parameter since we considered this parameter most relevant for CPAD design. In the future, this could be extended to wall shear stress maps or to detailed flow field analyses looking at recirculation areas, for example. In this study, we neglected PA and SVC anatomies, which may pose more complex hemodynamic boundary conditions depending on a patient's anatomical configuration. Due to their high shape variability (Fig. 1b), the generation of an average template shape of the entire TCPC geometry is difficult and may be focus of future studies. Further, we have approximated IVC inflow here as being time-invariant. Pulsatile flow may cause higher peak pressure drops, that however, can generally be neglected when simulating TCPC hemodynamics [44].

Here, we only assess the template graft hemodynamic performance. It is to be noted that future studies could focus on computing hemodynamic performance over a range of "synthetic" graft geometries, generated by combining the derived PCA shape modes and varying respective PCA shape mode loadings within realistic limits in order to obtain a larger number of possible scenarios. We believe however, that by using the average template graft as a representative of the population, a first step towards more realistic hemodynamic and geometric boundary conditions has been made.

Regarding the segmentation of complex cardiac anatomy such as the Fontan connection, operator-induced segmentation errors may occur. In this study we have used mostly automated tools applied by the same operator to minimize segmentation errors as much as possible. As many advanced segmentation procedures are currently being developed [45], we foresee a full automation of this process in the near future.

Europe PMC Funders Author Manuscripts

Finally, here we only look to the ECC graft as possible landing zone for a CPAD. Moving away from micro-axial pumps, recent studies focus on diamond shaped viscous impeller pumps that are to be deployed in the center of the TCPC junction [7,13,14,19]. We would like to emphasize that this study is meant to be exemplary for how to apply statistical shape modeling to cardiac device design. Thus, our approach can be applied to various types of anatomy and devices. We hope however, to have shown that statistical shape models and computed anatomical mean shapes provide a more realistic basis for device development and perform significantly better compared to simplified geometries when approximating population hemodynamics.

Conclusion

In this study, we assessed three-dimensional geometric variability of extra cardiac conduit grafts used in Fontan palliation via traditional morphometrics and statistical shape modeling. In a cohort of 18 patients, we report averages and confidence intervals of graft dimensions that could serve as boundary conditions for cavopulmonary assist device design. Graft length, curvature and diameter were found to be principal contributors to geometric variability and should be taken into account when assessing possible landing zones for cavopulmonary assist devices.

Furthermore, we computed the mean graft shape model as a representative of the challenging anatomical conditions in patients with the Fontan circulation. The model will be made available for device developers for improved *in-vitro* and *in-silico* testing of device deployment, fixation and hemodynamics. Using Computational Fluid Dynamics, we found the mean graft model to allow for a good approximation of average patient graft flow characteristics. To prove its superiority, we demonstrated and quantified for the first time that a computed mean graft model yields significantly less deviations from individual patient hemodynamics than a simplified tube geometry.

Our methodology combining statistical shape modeling with engineering analyses thus provides more realistic geometric and hemodynamic boundary conditions, which ultimately may allow improved and cost-effective cardiac device design in a “few-sizes-fits-all” fashion – whenever a patient-specific approach is not feasible.

Acknowledgment

MOCHA Collaborative Group: Andrew M. Taylor, Alessandro Giardini, Sachin Khambadkone, Silvia Schievano, Marc de Leval and T. -Y. Hsia (Institute of Cardiovascular Science, UCL, London, UK); Edward Bove and Adam Dorfman (University of Michigan, Ann Arbor, MI, USA); G. Hamilton Baker and Anthony Hlavacek (Medical University of South Carolina, Charleston, SC, USA); Francesco Migliavacca, Giancarlo Pennati and Gabriele Dubini (Politecnico di Milano, Milan, Italy); Alison Marsden (Stanford University, Stanford, CA, USA); Irene Vignon-Clementel (INRIA, Paris, France); Richard Figliola and John McGregor (Clemson University, Clemson, SC, USA).

Funding

The authors gratefully acknowledge support from Fondation Leducq (09CVD04), British Heart Foundation (Clinical Research Fellowship FS/12/35/29566), Engineering and Physical Sciences Research Council (EP/N02124X/1).

Europe PMC Funders Author Manuscripts

Nomenclature

3D	Three dimension(al)
bSSFP	Balanced, steady-state free precession CMR sequence
CFD	Computational Fluid Dynamics
CMR	Cardiovascular Magnetic Resonance
CO	Cardiac Output
CPAD	Cavopulmonary Assist Device
D_{av}	Average diameter along the centerline [mm]
$Dev_{template,i}$	Absolute deviation in pressure drop between the computed pressure drop of the template graft $\Delta p_{template}$ and the individual pressure drop $\Delta p_{graft,i}$ [%]
$Dev_{tube,i}$	Absolute deviation between the pressure drop of the simple tube Δp_{tube} and each individual pressure drop $\Delta p_{graft,i}$ [%]
D_{max}	Maximum diameter along the centerline [mm]
D_{min}	Minimum diameter along the centerline [mm]
ECC	Extra Cardiac Conduit
GPA	General Procrustes Approach
ICP	Iterative Closest Point algorithm
IVC	Inferior Vena Cava
LCL	Centerline length [mm]
LDDMM	Large Deformation Diffeomorphic Metric Mapping algorithm
LPA	Left Pulmonary Artery
PA	Pulmonary Artery
PCA	Principal Component Analysis
PC-MR	Phase-contrast magnetic resonance
ϕ_i	Set of deformation vectors, i.e. deformation function for each patient i
p_{outlet}	Static pressure at outlet [mmHg]
RPA	Right Pulmonary Artery

Europe PMC Funders Author Manuscripts

SD	Standard deviation
SSM	Statistical Shape Model
STL	Stereolithography
SV	Single Ventricle
SVC	Superior Vena Cava
TCPC	Total Cavopulmonary Connection
V	Volume [ml]
$\dot{V}_{in}$	Volume flux, inflow [l/min]
Δp	Pressure drop across graft [mmHg]
$\Delta p_{graft,i}$	Pressure drop across each individual patient graft i [mmHg]
$\Delta p_{template}$	Pressure drop across template graft [mmHg]
Δp_{tube}	Pressure drop across tube geometry [mmHg]
λ_V	Gaussian kernel width associated with deformation resolution
λ_W	Gaussian kernel width associated with shape resolution
μ	Viscosity [mPa s]
ρ	Density [kg/m^3]

References

[1]. Gewillig M. The Fontan Circulation. Heart. 2005; 91(6):839–846. [PubMed: 15894794]

[2]. Gersony WM. Fontan Operation After 3 Decades. Circulation. 2008; 117(1):13–15. [PubMed: 18172049]

[3]. Jaquiss RDB, Aziz H. Is Four Stage Management the Future of Univentricular Hearts? Destination Therapy in the Young. Semin Thorac Cardiovasc Surg Pediatr Card Surg Annu. 2016; 19(1):50–54. [PubMed: 27060043]

[4]. McRae MER. Long-term Issues After the Fontan Procedure. AACN Adv Crit Care. 2013; 24(3): 264–282. [PubMed: 23880749]

[5]. de Leval MR. The Fontan Circulation: What Have We Learned? What to Expect? Pediatr Cardiol. 1998; 19(4):316–320. [PubMed: 9636255]

[6]. Rodefeld MD, Boyd JH, Myers CD, LaLone BJ, Bezruczko AJ, Potter AW, Brown JW. Cavopulmonary assist: circulatory support for the univentricular fontan circulation. Ann Thorac Surg. 2003; 76(6):1911–1916. [PubMed: 14667610]

[7]. Delorme Y, Anupindi K, Kerlo AE, Shetty D, Rodefeld M, Chen J, Frankel S. Large eddy simulation of powered Fontan hemodynamics. J Biomech. 2013; 46(2):408–422. [PubMed: 23177085]

[8]. Haggerty CM, Fynn-Thompson F, McElhinney DB, Valente AM, Saikrishnan N, del Nido PJ, Yoganathan AP. Experimental and numeric investigation of Impella pumps as cavopulmonary

assistance for a failing Fontan. J Thorac Cardiovasc Surg. 2012; 144(3):563–569. [PubMed: 22336753]

[9]. Throckmorton AL, Kapadia JY, Chopski SG, Bhavsar SS, Moskowitz WB, Gullquist SD, Gangemi JJ, Haggerty CM, Yoganathan AP. Numerical, Hydraulic, and Hemolytic Evaluation of an Intravascular Axial Flow Blood Pump to Mechanically Support Fontan Patients. Ann Biomed Eng. 2010; 39(1):324–336. [PubMed: 20839054]

[10]. Throckmorton AL, Lopez-Isaza S, Moskowitz W. Dual-Pump Support in the Inferior and Superior Vena Cavae of a Patient-Specific Fontan Physiology. Artif Organs. 2013; 37(6):513–522. [PubMed: 23692310]

[11]. Lacour-Gayet FG, Lanning CJ, Stoica S, Wang R, Rech BA, Goldberg S, Shandas R. An Artificial Right Ventricle for Failing Fontan: In Vitro and Computational Study. Ann Thorac Surg. 2009; 88(1):170–176. [PubMed: 19559219]

[12]. Throckmorton AL, Ballman KK, Myers CD, Frankel SH, Brown JW, Rodefeld MD. Performance of a 3-Bladed Propeller Pump to Provide Cavopulmonary Assist in the Failing Fontan Circulation. Ann Thorac Surg. 2008; 86(4):1343–1347. [PubMed: 18805191]

[13]. Rodefeld MD, Coats B, Fisher T, Giridharan GA, Chen J, Brown JW, Frankel SH. Cavopulmonary assist for the univentricular Fontan circulation: von Kármán viscous impeller pump. J Thorac Cardiovasc Surg. 2010; 140(3):529–536. [PubMed: 20561640]

[14]. Kennington JR, Frankel SH, Chen J, Koenig SC, Sobieski MA, Giridharan GA, Rodefeld MD. Design Optimization and Performance Studies of an Adult Scale Viscous Impeller Pump for Powered Fontan in an Idealized Total Cavopulmonary Connection. Cardiovasc Eng Technol. 2011; 2(4):237–243.

[15]. Giridharan GA, Koenig SC, Kennington J, Sobieski MA, Chen J, Frankel SH, Rodefeld MD. Performance evaluation of a pediatric viscous impeller pump for Fontan cavopulmonary assist. J Thorac Cardiovasc Surg. 2013; 145(1):249–257. [PubMed: 22421403]

[16]. Valdovinos J, Shkolyar E, Carman GP, Levi DS. In Vitro Evaluation of an External Compression Device for Fontan Mechanical Assistance. Artif Organs. 2014; 38(3):199–207. [PubMed: 24147904]

[17]. Yamada, A., Shiraishi, Y., Miura, H., Yambe, T., Omran, MH., Shiga, T., Tsuboko, Y., Homma, D., Yamagishi, M. Peristaltic hemodynamics of a new pediatric circulatory assist system for Fontan circulation using shape memory alloy fibers. 2013 35th Annual International Conference of the IEEE Engineering in Medicine and Biology Society (EMBC); 2013. p. 683-686.

[18]. KrishnankuttyRema R, Dasi LP, Pekkan K, Sundareswaran K, Fogel M, Sharma S, Kanter K, Spray T, Yoganathan AP. Quantitative Analysis of Extracardiac Versus Intraatrial Fontan Anatomic Geometries. Ann Thorac Surg. 2008; 85(3):810–817. [PubMed: 18291147]

[19]. Giridharan GA, Ising M, Sobieski MA, Koenig SC, Chen J, Frankel S, Rodefeld MD. Cavopulmonary assist for the failing Fontan circulation: Impact of ventricular function on mechanical support strategy. ASAIO J Am Soc Artif Intern Organs 1992. 2014; 60(6):707–715.

[20]. Dasi LP, Sundareswaran KS, Sherwin C, de Zelicourt D, Kanter K, Fogel MA, Yoganathan AP. Larger aortic reconstruction corresponds to diminished left pulmonary artery size in patients with single-ventricle physiology. J Thorac Cardiovasc Surg. 2010; 139(3):557–561. [PubMed: 19880146]

[21]. Young AA, Frangi AF. Computational cardiac atlases: from patient to population and back. Exp Physiol. 2009; 94(5):578–596. [PubMed: 19098087]

[22]. Farrar G, Suinesiaputra A, Gilbert K, Perry JC, Hegde S, Marsden A, Young AA, Omens JH, McCulloch AD. Atlas-based ventricular shape analysis for understanding congenital heart disease. Prog Pediatr Cardiol. 2016; 43:61–69. [PubMed: 28082823]

[23]. Yushkevich PA, Piven J, Hazlett HC, Smith RG, Ho S, Gee JC, Gerig G. User-guided 3D active contour segmentation of anatomical structures: Significantly improved efficiency and reliability. NeuroImage. 2006; 31(3):1116–1128. [PubMed: 16545965]

[24]. Antiga L, Piccinelli M, Botti L, Ene-Iordache B, Remuzzi A, Steinman DA. An image-based modeling framework for patient-specific computational hemodynamics. Med Biol Eng Comput. 2008; 46(11):1097–1112. [PubMed: 19002516]

[25]. Piccinelli M, Veneziani A, Steinman DA, Remuzzi A, Antiga L. A Framework for Geometric Analysis of Vascular Structures: Application to Cerebral Aneurysms. IEEE Trans Med Imaging. 2009; 28(8):1141–1155. [PubMed: 19447701]

[26]. Antiga L, Steinman DA. Robust and objective decomposition and mapping of bifurcating vessels. IEEE Trans Med Imaging. 2004; 23(6):704–713. [PubMed: 15191145]

[27]. Durrleman S, Prastawa M, Charon N, Korenberg JR, Joshi S, Gerig G, Trouvé A. Morphometry of anatomical shape complexes with dense deformations and sparse parameters. NeuroImage. 2014; 101:35–49. [PubMed: 24973601]

[28]. Durrleman S, Pennec X, Trouvé A, Ayache N. Statistical models of sets of curves and surfaces based on currents. Med Image Anal. 2009; 13(5):793–808. [PubMed: 19679507]

[29]. Bruse JL, Cervi E, McLeod K, Biglino G, Sermesant M, Pennec X, Taylor AM, Schievano S, Hsia T-Y. Looks do matter! Aortic arch shape following hypoplastic left heart syndrome palliation correlates with cavopulmonary outcomes. Ann Thorac Surg. 2016

[30]. Beg MF, Miller MI, Trouvé A, Younes L. Computing Large Deformation Metric Mappings via Geodesic Flows of Diffeomorphisms. Int J Comput Vis. 2005; 61(2):139–157.

[31]. Bruse JL, McLeod K, Biglino G, Ntsinjana HN, Capelli C, Hsia T-Y, Sermesant M, Pennec X, Taylor AM, Schievano S. A statistical shape modelling framework to extract 3D shape biomarkers from medical imaging data: assessing arch morphology of repaired coarctation of the aorta. BMC Med Imaging. 2016; 16:40. [PubMed: 27245048]

[32]. Besl PJ, McKay ND. A method for registration of 3-D shapes. IEEE Trans Pattern Anal Mach Intell. 1992; 14(2):239–256.

[33]. Gower JC. Generalized procrustes analysis. Psychometrika. 1975; 40(1):33–51.

[34]. Jolliffe, IT. Principal Component Analysis. Springer-Verlag New York, Inc; 2002.

[35]. Mansi, T., Durrleman, S., Bernhardt, B., Sermesant, M., Delingette, H., Voigt, I., Lurz, P., Taylor, AM., Blanc, J., Boudjemline, Y., Pennec, X., et al. A Statistical Model of Right Ventricle in Tetralogy of Fallot for Prediction of Remodelling and Therapy Planning. Medical Image Computing and Computer-Assisted Intervention – MICCAI 2009. Yang, G-Z.Hawkes, D.Rueckert, D.Noble, A., Taylor, C., editors. Springer Berlin Heidelberg; 2009. p. 214-221.

[36]. Mansi T, Voigt I, Leonardi B, Pennec X, Durrleman S, Sermesant M, Delingette H, Taylor AM, Boudjemline Y, Pongiglione G, Ayache N. A Statistical Model for Quantification and Prediction of Cardiac Remodelling: Application to Tetralogy of Fallot. IEEE Trans Med Imaging. 2011; 30(9):1605–1616. [PubMed: 21880565]

[37]. Ahrens J, Geveci B, Law C. ParaView: An End-User Tool for Large-Data Visualization. Vis Handb. 2005:717.

[38]. Rogers LS, Glatz AC, Ravishankar C, Spray TL, Nicolson SC, Rychik J, Rush CH, Gaynor JW, Goldberg DJ. 18 Years of the Fontan Operation at a Single Institution: Results From 771 Consecutive Patients. J Am Coll Cardiol. 2012; 60(11):1018–1025. [PubMed: 22818071]

[39]. Lee C, Lee C-H, Hwang SW, Lim HG, Kim S-J, Lee JY, Shim W-S, Kim W-H. Midterm follow-up of the status of Gore-Tex graft after extracardiac conduit Fontan procedure. Eur J Cardiothorac Surg. 2007; 31(6):1008–1012. [PubMed: 17419069]

[40]. Ochiai Y, Imoto Y, Sakamoto M, Kajiwara T, Sese A, Watanabe M, Ohno T, Joo K. Mid-term follow-up of the status of Gore-Tex graft after extracardiac conduit Fontan procedure. Eur J Cardiothorac Surg. 2009; 36(1):63–68. [PubMed: 19329333]

[41]. McGregor, R., Szczerba, D., von Siebenthal, M., Muralidhar, K., Székely, G. Exploring the Use of Proper Orthogonal Decomposition for Enhancing Blood Flow Images Via Computational Fluid Dynamics. Medical Image Computing and Computer-Assisted Intervention - MICCAI 2008. Metaxas, D.Axel, L.Fichtinger, G., Székely, G., editors. Springer Berlin Heidelberg; 2008. p. 782-789.

[42]. Guibert R, McLeod K, Caiazzo A, Mansi T, Fernández MA, Sermesant M, Pennec X, Vignon-Clementel IE, Boudjemline Y, Gerbeau J-F. Group-wise construction of reduced models for understanding and characterization of pulmonary blood flows from medical images. Med Image Anal. 2014; 18(1):63–82. [PubMed: 24148257]

[43]. Beier S, Ormiston J, Webster M, Cater J, Norris S, Medrano-Gracia P, Young A, Cowan B. Impact of bifurcation angle and other anatomical characteristics on blood flow – A computational

study of non-stented and stented coronary arteries. J Biomech. 2016; 49(9):1570–1582. [PubMed: 27062590]

[44]. Haggerty CM, Restrepo M, Tang E, de Zélicourt DA, Sundareswaran KS, Mirabella L, Bethel J, Whitehead KK, Fogel MA, Yoganathan AP. Fontan hemodynamics from 100 patient-specific cardiac magnetic resonance studies: A computational fluid dynamics analysis. J Thorac Cardiovasc Surg. 2014; 148(4):1481–1489. [PubMed: 24507891]

[45]. Zuluaga MA, Burgos N, Mendelson AF, Taylor AM, Ourselin S. Voxelwise atlas rating for computer assisted diagnosis: Application to congenital heart diseases of the great arteries. Med Image Anal. 2015; 26(1):185–194. [PubMed: 26433929]

Europe PMC Funders Author Manuscripts

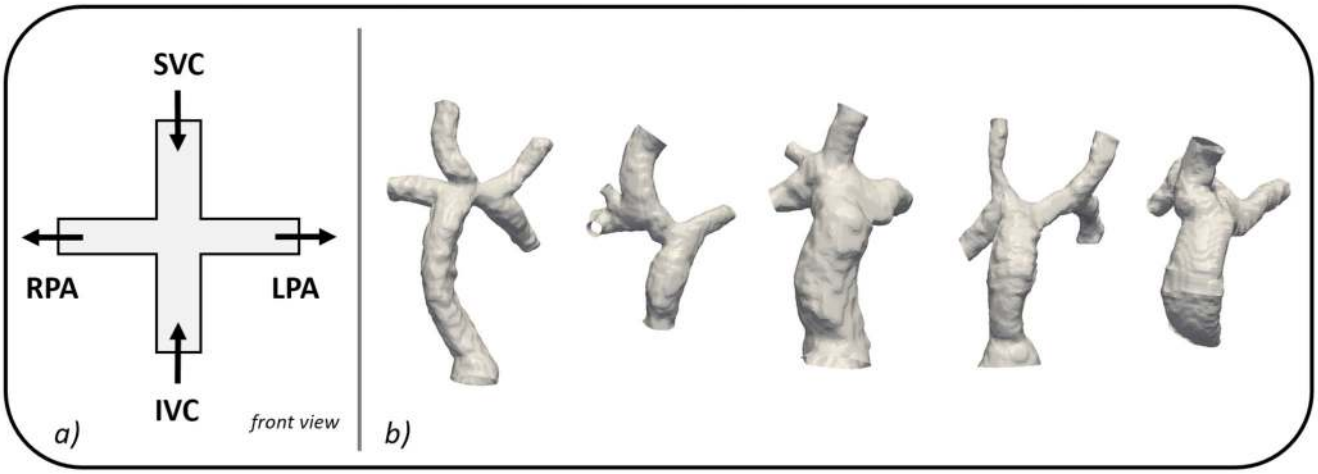

Fig. 1.

Europe PMC Funders Author Manuscripts

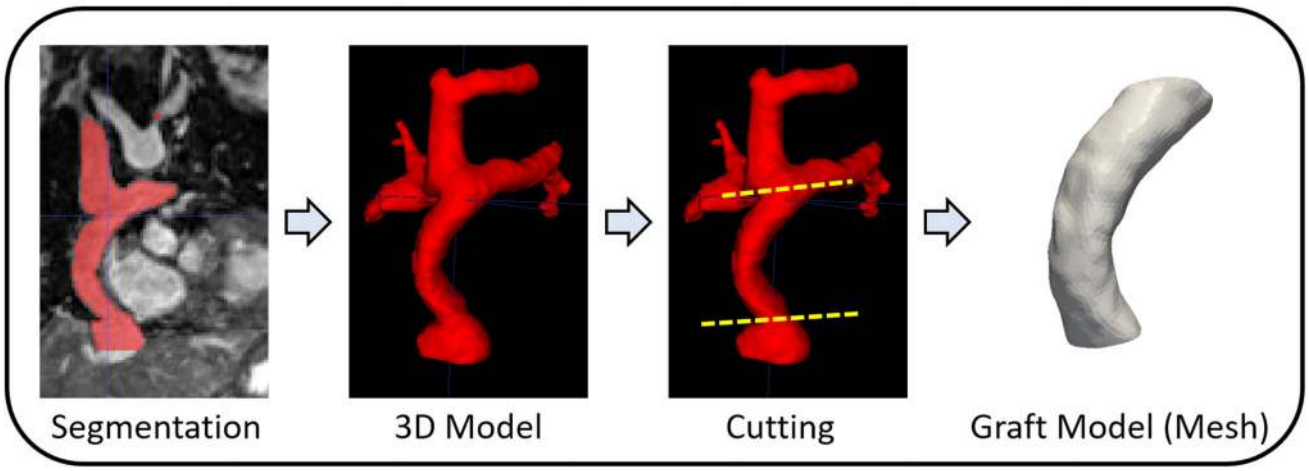

Fig. 2.

Europe PMC Funders Author Manuscripts

Europe PMC Funders Author Manuscripts

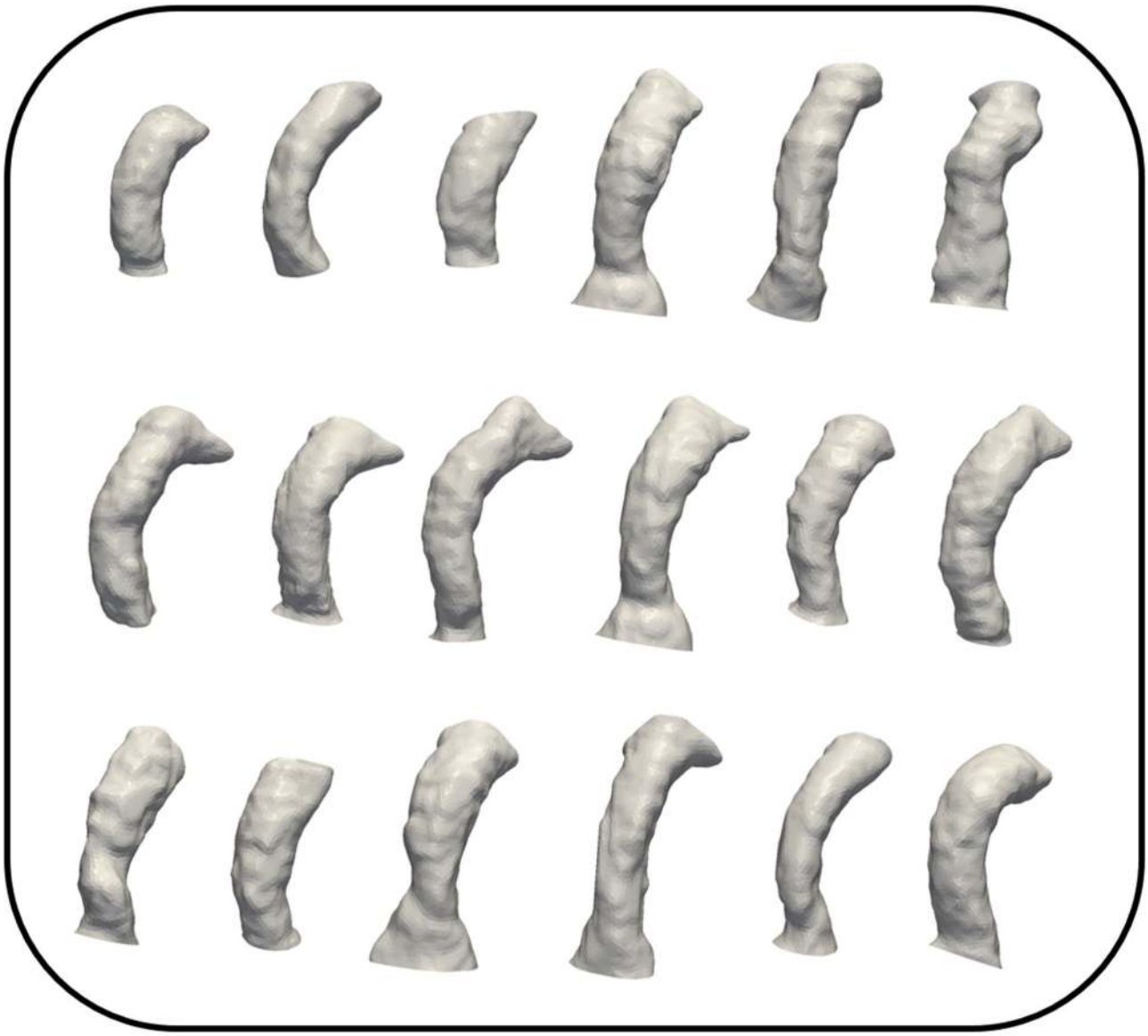

Fig. 3.

Europe PMC Funders Author Manuscripts

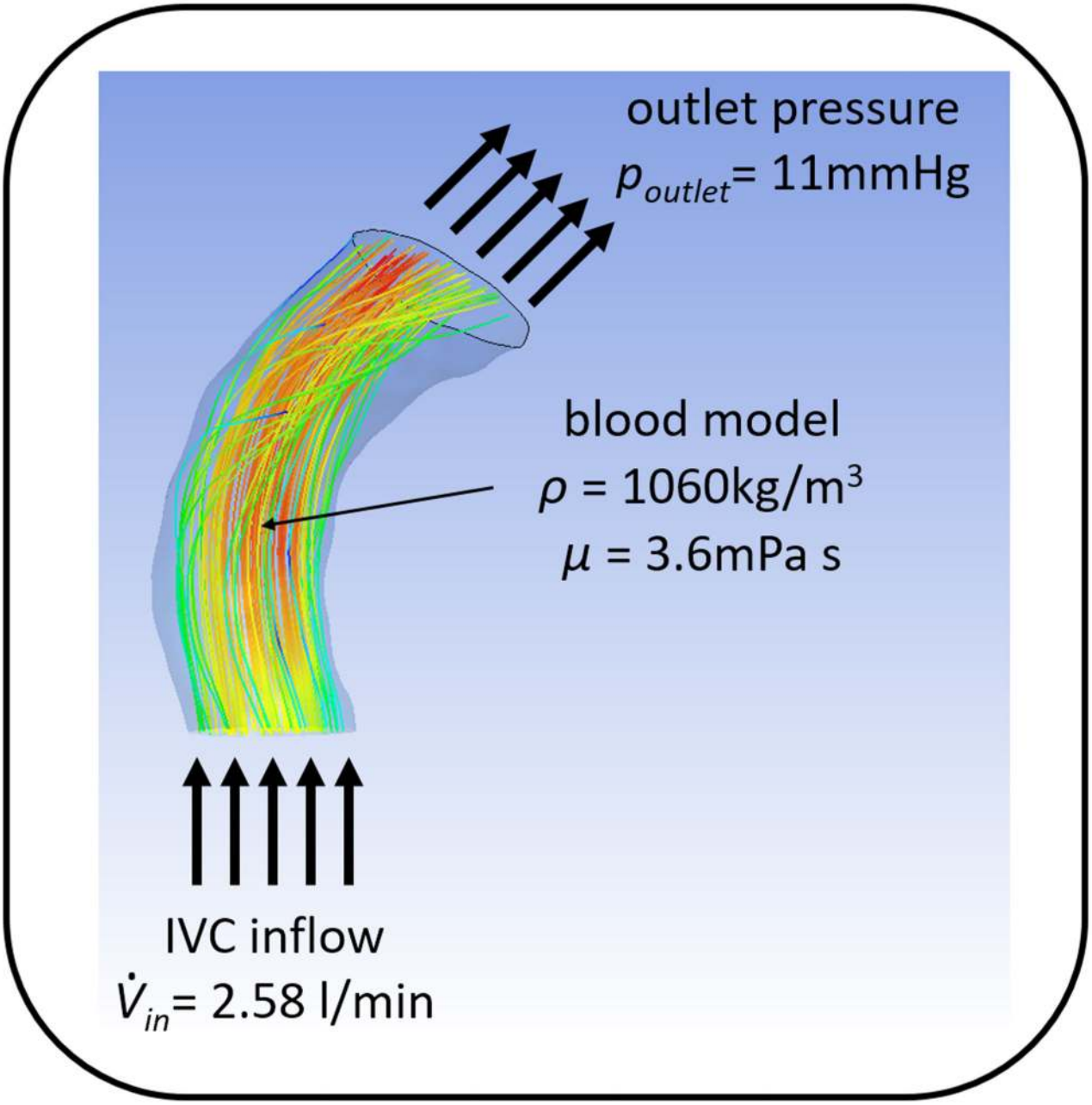

Fig. 4.

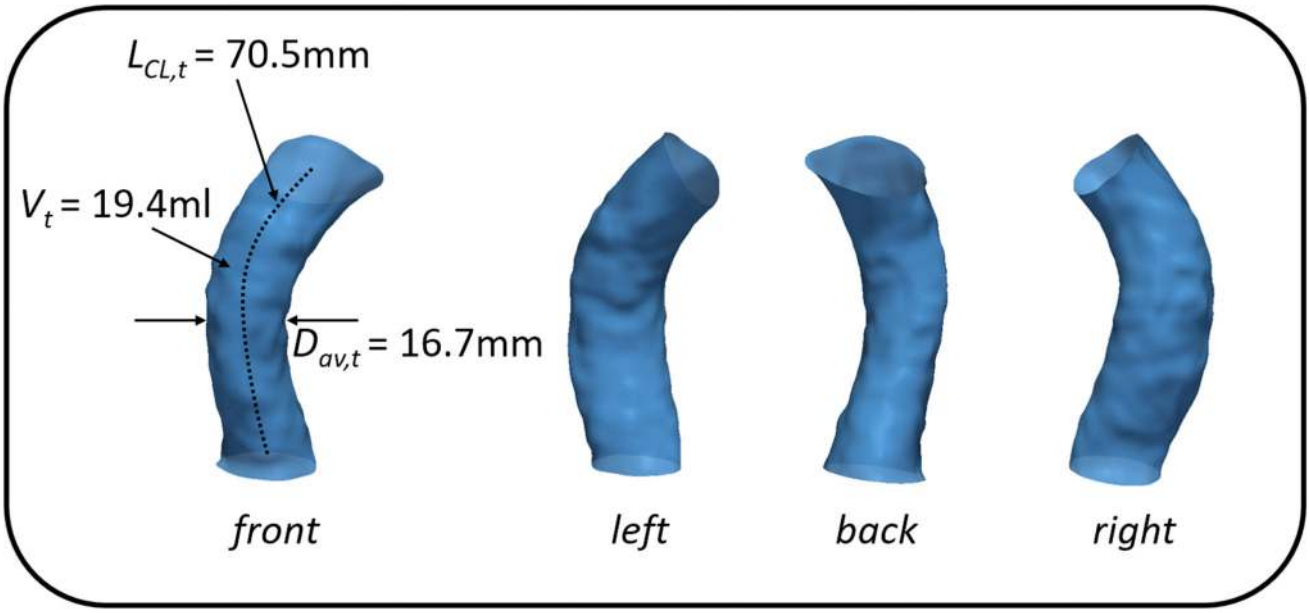

Fig. 5.

Europe PMC Funders Author Manuscripts

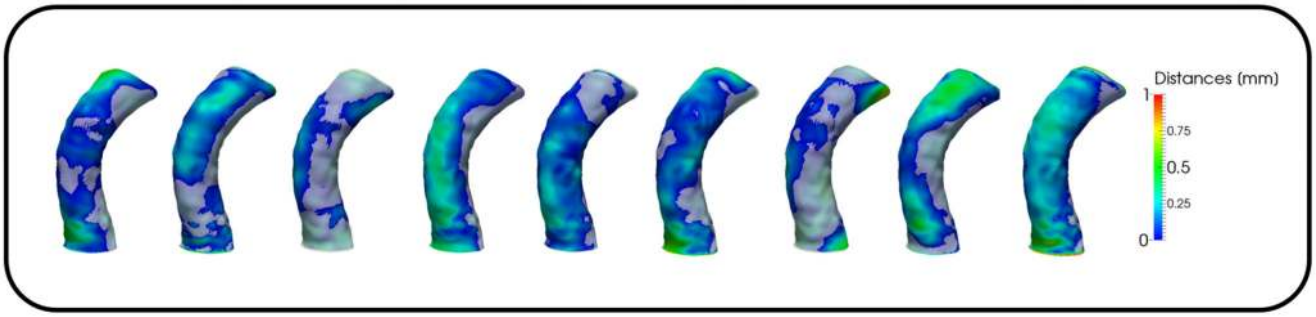

Fig. 6.

Europe PMC Funders Author Manuscripts

Europe PMC Funders Author Manuscripts

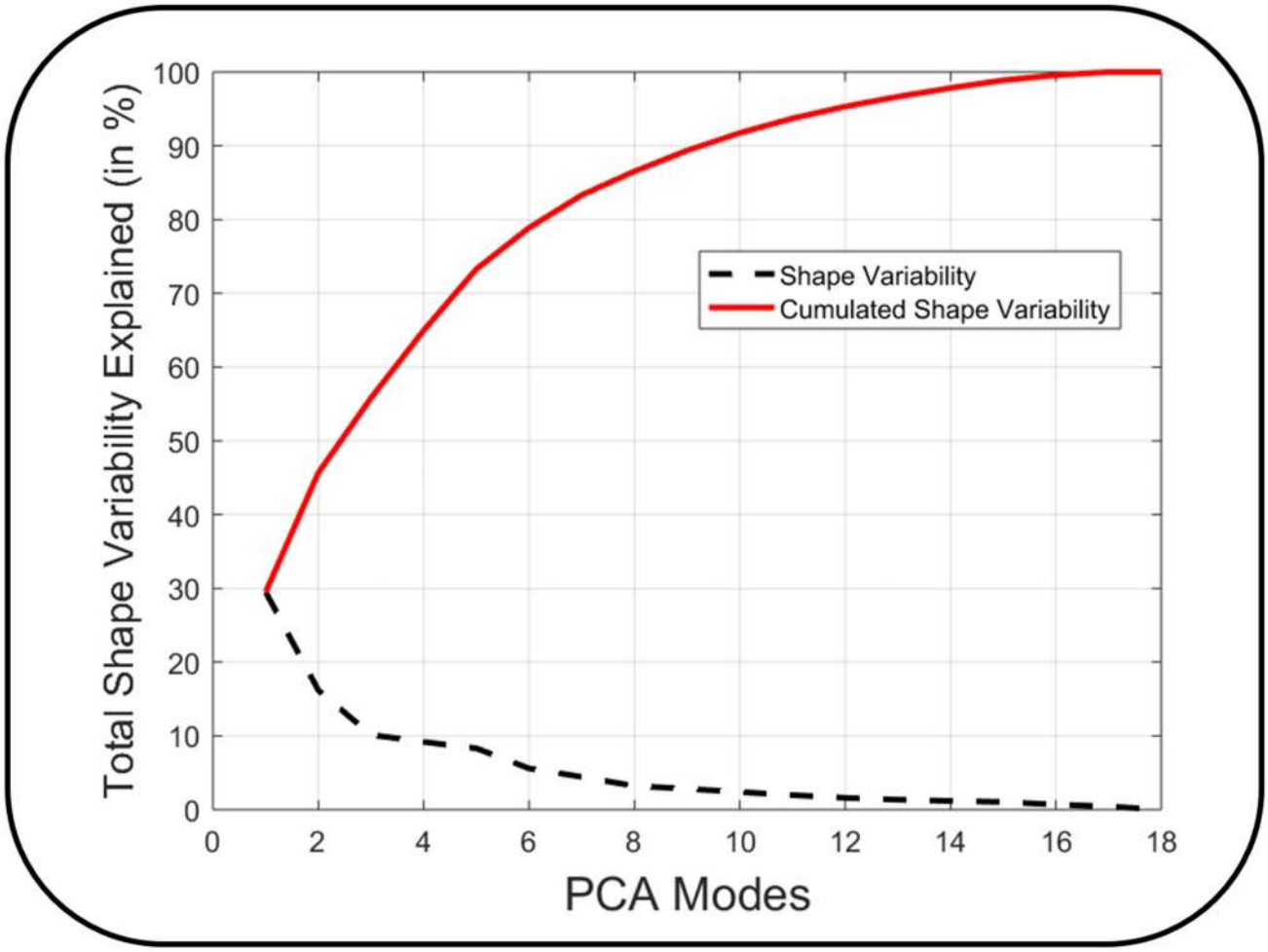

Fig. 7.

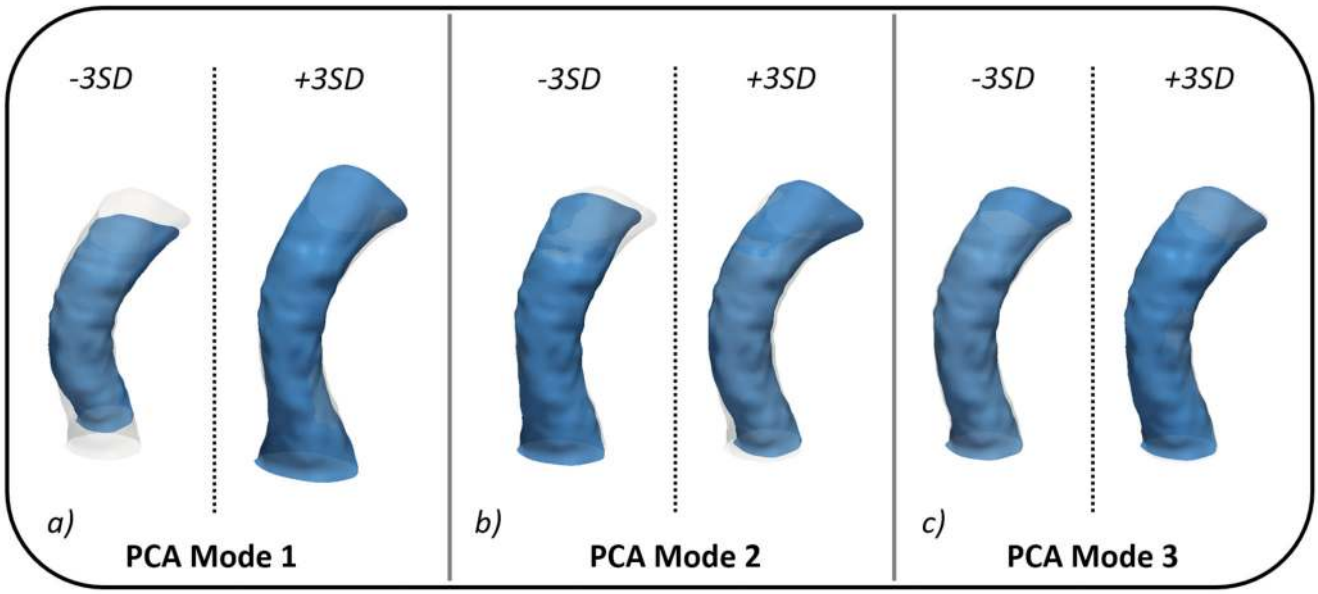

Fig. 8.

Europe PMC Funders Author Manuscripts

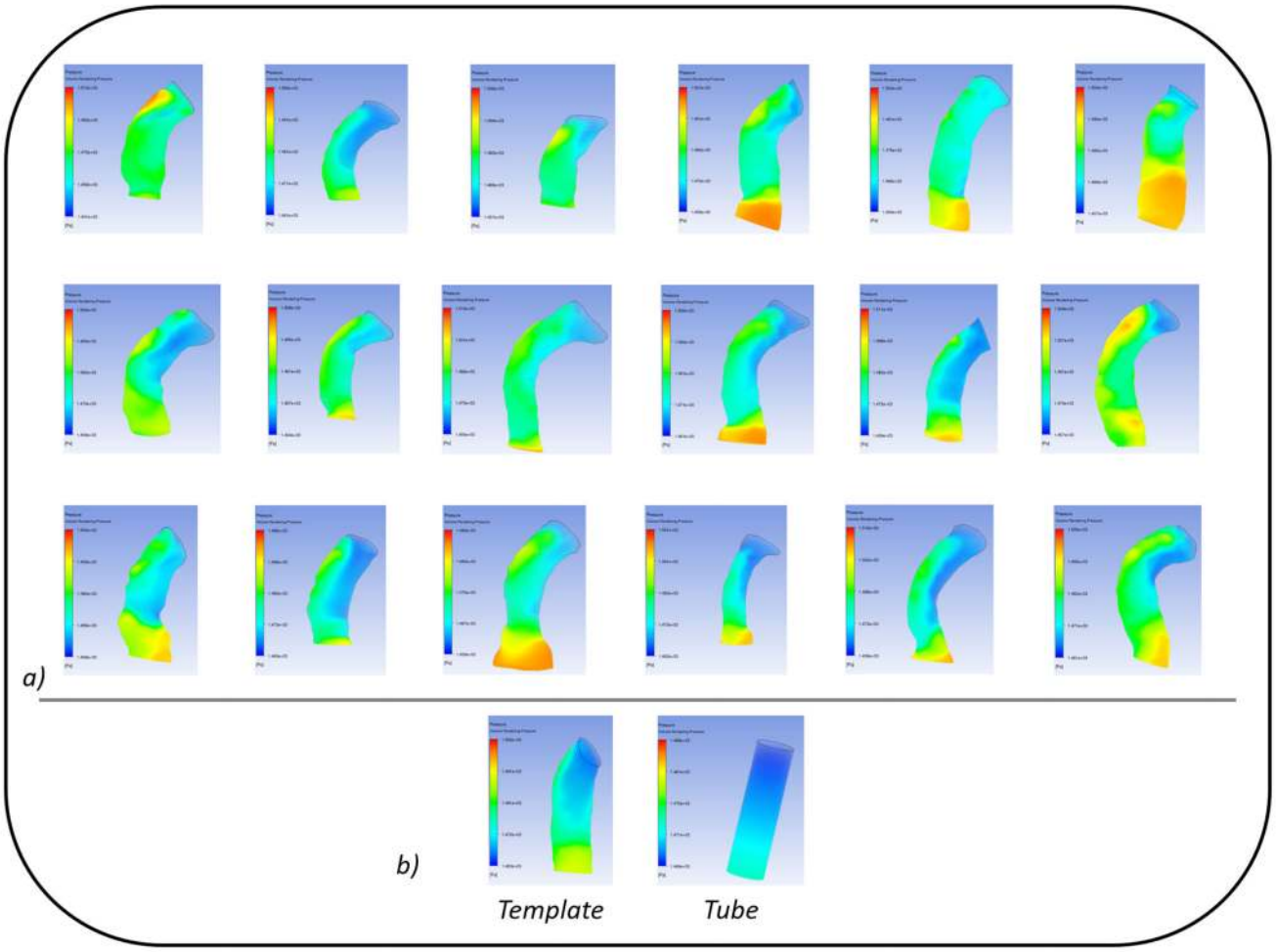

Fig. 9.

Europe PMC Funders Author Manuscripts

Europe PMC Funders Author Manuscripts

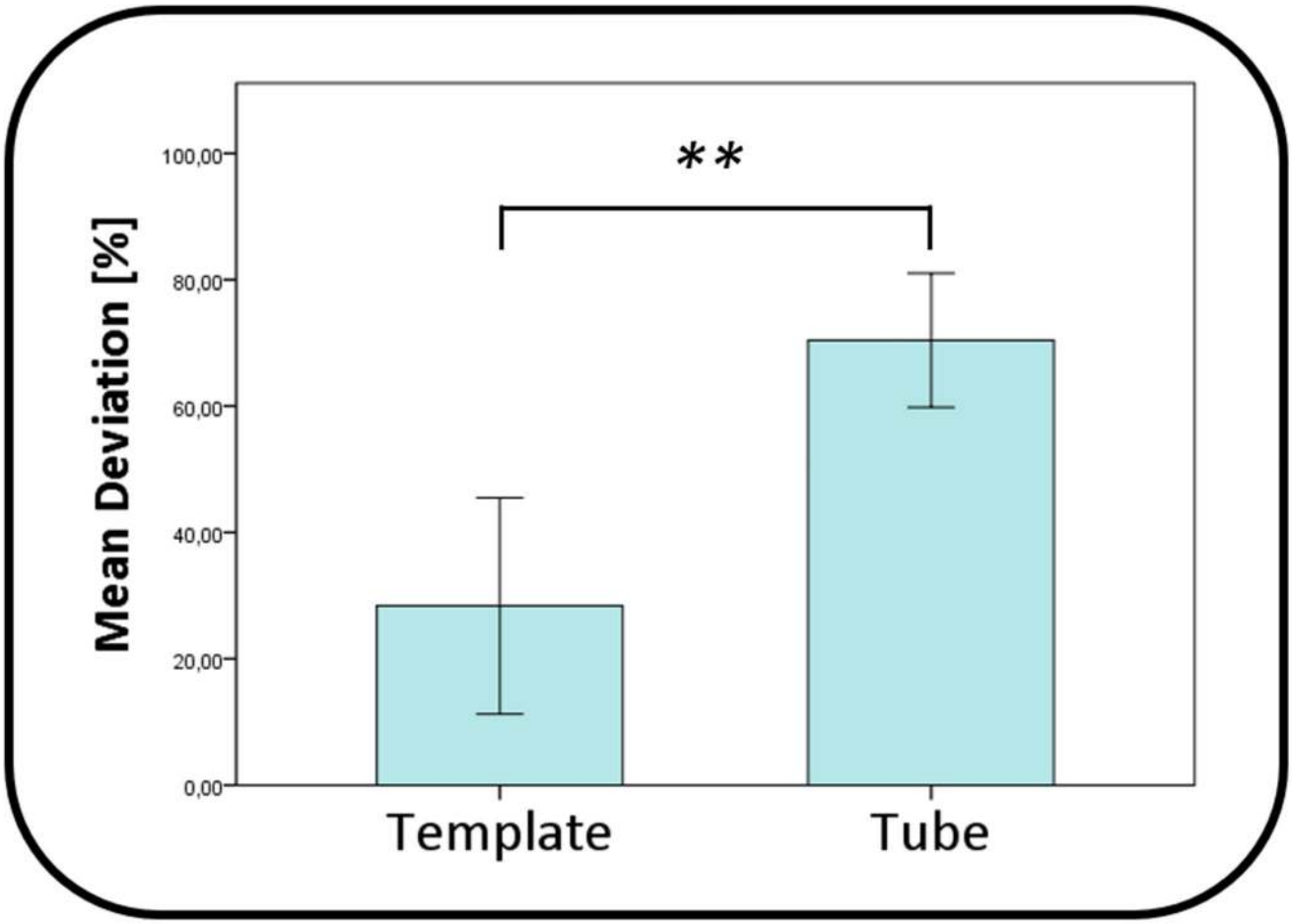

Fig. 10.

Europe PMC Funders Author Manuscripts

Table 1

ID	Sex	Age at CMR [years]	Primary Diagnosis	IVC Flow [l/min]
Patient 1	m	5.30	Multiple VSD	0.7
Patient 2	m	26.3	HLHS	2.3
Patient 3	m	16.4	DORV	1.7
Patient 4	m	15.3	MA	1.5
Patient 5	m	18.0	DORV	3.6
Patient 6	f	19.7	HLHS	4.4
Patient 7	m	14.8	DILV	3.8
Patient 8	m	11.8	TA	2.5
Patient 9	m	17.4	TA	4.4
Patient 10	m	15.3	DORV, MA, PS	1.5
Patient 11	f	15.8	PA IVS	3.5
Patient 12	f	16.6	HRHS, PA IVS	1.8
Patient 13	m	14.5	PA IVS	1.9
Patient 14	m	12.9	TA	1.4
Patient 15	m	15.8	PA IVS	3.5
Patient 16	m	17.0	HLHS	2.4
Patient 17	m	15.9	TA, PA	2.9
Patient 18	m	16.2	TA	2.6

Europe PMC Funders Author Manuscripts

Table 2

ID	L_{CL} [mm]	L_t	C_{av}	V [ml]	D_{max} [mm]	D_{min} [mm]	D_{av} [mm]	Δp_{graft} [mmHg]	Dev_{mean} [%]	Dev_{tube} [%]
Patient 1	51.5	0.097	0.213	11.7	16.6	14.6	16.0	0.084	78.9	39.9
Patient 2	63.1	0.141	0.215	16.8	16.5	13.0	15.1	0.131	14.4	61.5
Patient 3	47.4	0.054	0.256	11.1	17.6	15.0	16.5	0.122	22.6	58.8
Patient 4	76.6	0.097	0.233	24.4	19.0	14.5	17.0	0.219	31.5	77.0
Patient 5	81.1	0.078	0.283	23.3	19.2	13.2	16.1	0.199	24.8	74.7
Patient 6	73.0	0.075	0.201	24.5	22.7	15.4	18.2	0.209	28.2	75.9
Patient 7	72.2	0.224	0.274	19.5	17.7	15.7	16.4	0.151	0.60	66.6
Patient 8	67.5	0.195	0.227	17.1	17.0	14.3	15.5	0.204	26.3	75.2
Patient 9	97.7	0.359	0.232	21.0	17.2	13.0	15.3	0.251	40.3	80.0
Patient 10	80.0	0.111	0.172	24.8	19.4	14.2	16.2	0.216	30.6	76.7
Patient 11	63.4	0.088	0.195	14.9	17.0	13.3	15.2	0.230	34.7	78.0
Patient 12	83.6	0.198	0.456	22.1	17.5	12.5	16.1	0.229	34.5	78.0
Patient 13	63.3	0.071	0.220	18.9	18.5	12.4	15.5	0.185	19.0	72.8
Patient 14	58.8	0.086	0.202	17.0	19.0	15.3	17.5	0.113	32.3	55.6
Patient 15	76.7	0.081	0.211	29.1	22.1	13.1	18.4	0.157	4.60	68.0
Patient 16	78.4	0.059	0.281	21.9	18.5	14.1	15.8	0.200	25.1	74.8
Patient 17	72.0	0.115	0.254	17.2	16.3	11.8	14.1	0.281	46.7	82.1
Patient 18	77.0	0.224	3.884	23.7	18.5	16.6	17.7	0.178	15.6	71.7
MEAN	**71.3**	**0.131**	**0.445**	**19.9**	**18.4**	**14.0**	**16.3**	**0.187**	**28.4**	**70.4**
STD	**12.1**	**0.080**	**0.860**	**4.80**	**1.80**	**1.30**	**1.10**	**0.052**	**17.1**	**10.6**

Europe PMC Funders Author Manuscripts

Table 3

ID	L_{CL} [mm]	V [ml]	D_{max} [mm]	D_{min} [mm]	D_{av} [mm]	Δp [mmHg]
Population Mean	71.3	19.9	18.4	14.0	16.3	0.187
Template	70.5	19.4	17.8	15.8	16.8	0.150
Tube	70.5	22.2	20.0	20.0	20.0	0.050

Europe PMC Funders Author Manuscripts

Table 4

Parameter	PCA Shape Mode 1	PCA Shape Mode 2	PCA Shape Mode 3
L_{CL} *[mm]*	**<.001****	.094	.941
L_t	.570	**.001****	.426
C_{av}	.344	**.045***	.733
V [ml]	**<.001****	.550	.326
D_{max} *[mm]*	**.009****	**.004****	.677
D_{min} *[mm]*	.387	.308	.410
D_{av} *[mm]*	.478	**.013***	.099